FAST: A combined NOC and Transient Fuel Model for CANDU fuel

A. Prudil¹, B.J. Lewis¹, P.K. Chan^{1*}, and J.J. Baschuk²

¹Royal Military College of Canada, Kingston, Ontario, Canada

*Department of Chemistry and Chemical Engineering

PO Box 17000, Station Forces

Kingston, Ontario CANADA, K7K 7B4

613-541-6000 x6145, Paul.Chan@rmc.ca

²Atomic Energy of Canada Limited (AECL), Chalk River, Ontario, Canada

ABSTRACT – The Fuel And Sheath modelling Tool (FAST) is a fuel performance code that is being developed for both normal and transient operating conditions. FAST includes models for heat generation and transport, thermal-expansion, elastic strain, densification, fission product swelling, pellet relocation, contact, grain growth, fission gas release, gas and coolant pressure and sheath creep. These models have been implemented using the Comsol finite-element platform. The equations are solved on a two-dimensional (radial-axial) geometry of a fuel pellet and sheath. FAST has undergone a proof of concept validation against experimental data and comparison to the ELESTRES and ELOCA fuel performance codes. The results show excellent agreement with experimental measurements and the above stated IST- codes.

Introduction

Nuclear fuel design is a key component of the design of new reactors, improve the performance of existing reactors, and mitigate reactor aging phenomena. Computer modeling tools with predictive capability are necessary to assess new designs to support fuel qualification. This is accomplished primarily by minimizing the economic cost and difficulty associated with performing in-reactor measurements. These tools, in effect, act as advanced interpolation (and in some cases extrapolation) tools to help bridge the gaps between the application (power reactors) and the experimental results (in- and out-reactor experiments).

Like all other computer models, nuclear-fuel modelling codes must always be designed to accommodate the finite computing resources available to them. This has historically favoured the development of fuel modelling codes employing one-dimensional or quasi-two-dimensional representations of fuel-element geometry to reduce the computation expense of the models to manageable levels. The complexity of these models was further reduced by separating the codes for modeling into long and short time-scale phenomena. This fuel modeling paradigm has been employed for the LWR fuel modeling codes FRAPCON+FRAPTRAN [1] as well as the CAUDU ELESTRES+ELOCA [2,3] codes (previously ELESIM+ELOCA).

In the time since these models were first developed, advancements in both computer hardware and software have expanded modelling capabilities. This advancement has made feasible more computationally expensive models which require fewer simplifying assumptions. The more computationally expensive models have the potential of greater predictive capabilities, more mechanistic models, and more diverse feature sets than those previously available. This has led to the development of a new fuel modeling paradigm employing features such as coupled multi-dimensional, multiphysics techniques and unification of normal and transient modeling domains

12th International Conference on CANDU Fuel

Holiday-Inn Waterfront Hotel Kingston, Ontario, Canada, 2013 September 15-18

into a single code. There are numerous examples of codes with one or more of these features, such as FALCON [4], TRANSURANUS [5,6], FEMAXI [7], and BISON [8,9].

A common trait of most codes is that they have been developed as purpose-built, standalone, computer programs in which the physical models are developed as part of the numerical methods directly in the source code. This architecture offers some advantages, particularly in terms of computational efficiency, protection of intellectual property, and guarding against accidental modification. However, the hard-coded nature of these code makes them time consuming to modify. This may limit their application for research and design needs which may require modification of the model geometry, material properties, mathematical descriptions of phenomena, or application of different initial or boundary conditions.

An alternate architecture has also emerged which provides greater separation of the modeling tasks from the numerical solution tasks. The two main advantages of this architecture is the potential reduction in the difficulty associated with modifying the model, and the ability to use an existing numerical solution infrastructure. This is the methodology employed by the FAST code (the subject of this work) and the BISION code.

The FAST model has been developed on the Comsol Multiphysics (v.4.3a) finite-element platform. Significant reduction in development time and cost can be achieved compared to a stand-alone in-house code architecture by utilizing commercially available pre-and-post-processing tools for various tasks such as building model geometry and finite-element meshes, solving linear systems and graphing results, rather than developing custom tools for the same task. The Comsol Multiphysics platform is extremely flexible, allowing the solution to a wide range of ordinary, and partial differential equations with arbitrary coupling of the dependent variables. The discretization process for numerical solution is accomplished automatically as part of the solution process. Thus, it is able to use standard mathematical representations of the equations already familiar to scientist and engineers.

The FAST code is a collection of separate effects models (both mechanistic and empirical) coupled together to obtain a simultaneous solution using the Comsol platform. This model has evolved from previous fully-coupled two-dimensional (radial-axial) models developed at the Royal Military College of Canada (RMC) [10,11]. The FAST code has three broad motivations, which have guided the design decisions:

- Improve prediction of sheath strain including circumferential ridging effects in support of Iodine Induced Stress Corrosion Cracking models
- Serve as a research tool, to be adapted to applications as needed for advanced fuel design and modeling and prototyping new phenomena models
- Serve as a testing platform for designing future fuel modeling codes for use in safety and licensing applications in Canada

The Section 1 of this paper outlines some of the key theory employed in the FAST code. Section 2 presents a proof of concept validation of the FAST model with comparisons to experimental measurements and Canadian industry standard codes. A discussion of the results is provided in Section 3.

1. Model Development

The behavior of nuclear fuel during irradiation is a complicated multi-physics problem involving many branches of science and engineering. In the following subsections the separate effects models used in the FAST code have been summarized. In the interest of brevity, the material property models have not been included. These have been are taken from Atomic Energy of Canada Limited (AECL), MATerial PROperties for light-water reactor analysis (MATPRO) and journal publications.

1.1 Model Geometry

The model geometry consists of one half-pellet in the radial-axial plane (axisymmetric) with an accompanying sheath. This includes options for central holes as well as dishing and chamfering of one or both ends of the pellet. The model currently assumes that the single pellet is representative of all pellets within the element (no strong axial dependence of the boundary conditions). This allows a periodic boundary condition to be applied which bounds the model in the axial direction. It is worth noting that the geometry can be modified in the COMSOL Graphical User Interface (GUI) as needed.

1.2 Heat Generation & Transport

The primary requirement of any fuel modelling code is to determine the temperature, T, throughout the fuel element because most material properties are temperature dependent and many phenomena are thermally driven. Heat transport in solid components is modelled by the heat-conduction equation:

$$\rho C_p \frac{\partial T}{\partial t} = \nabla \cdot (k \nabla T) + Q_{prod} \tag{1}$$

where ρ , C_p and k are the material properties of density, specific heat capacity and thermal conductivity, respectively. These are not constants; they are dependent on many factors such as temperature, porosity, burnup, radiation damage and/or manufacturing conditions. These dependencies are accounted for using empirical and semi-empirical correlations. The volumetric heat production rate, Q_{prod} , accounts for heat produced in the fuel. The FAST model assumes this quantity to be proportional to the thermal neutron flux in the fuel. The flux model employed in the code was taken from ELESTRES-IST [2]. This model is a correlation obtained by curve-fitting flux profile predictions from reactor physics simulations. The thermal neutron flux profile in this model is given by

$$Q_{prod} = f_{mag} \left(I_0 \left(\kappa_{flux} r \right) + \beta_{flux} e^{\lambda_{flux} (r - P_r)} \right)$$
 (2).

Here f_{mag} is a proportionality coefficient to achieve the required average linear power for the element, I_0 is the zeroth order modified-Bessel function of the first kind, r is the radial coordinate, P_r is the pellet radius, and the parameters κ_{flux} , β_{flux} , and λ_{flux} are the flux depression parameters derived and tabulated from the reactor physics codes as a function of initial pellet radius, enrichment and average burnup. Note that these parameters are dependent on the neutron spectrum and therefore should be updated for other reactor designs .

Heat transport across the pellet-to-sheath gap is modelled assuming one-dimensional steady-state heat transfer due to the high aspect ratio. The radial heat flux is given by

$$Q_r = \left(h_{gap,gas} + h_{gap,solid} + h_{gap,rad}\right) \left(T_{fuel} - T_{sheath}\right) \tag{3}$$

where the heat transfer coefficients, h_{gap} , are associated with gaseous conduction, solid-to-solid surface conduction and radiative heat-transfer respectively. The gaseous and the solid-solid coefficients are obtained from the model of Campbell et al. [12]:

$$h_{gap,gas} = \frac{k_g}{1.5(R_f + R_s) + d_{gap} + g}$$
 (4)

$$h_{gap,solid} = \left(\frac{2k_f k_s}{k_f + k_s}\right) \left(\frac{1}{a_0 H}\right) \sqrt{\frac{P_i}{d_{gap}}}$$
 (5).

The variables k_g , k_f and k_s are the thermal conductivity of the gas at the fuel and sheath, respectively. The average local gap distance is denoted by d_{gap} , which is effectively increased by the surface roughness of the fuel and sheath materials, R_f , R_s , and the temperature jump distances at the surfaces, g. In the solid-to-solid conductance term, a_o is a constant with a value of $8.6 \cdot 10^{-9}$ m^{0.5} Pa^{0.5}, P_i is the local average contact pressure at the interface and H is the Meyer hardness of the Zircaloy. In the case of an open gap, the contact pressure is zero and the solid conduction term does not contribute. The radiative heat flux is calculated assuming grey body radiation between parallel surfaces. This yields a heat transfer coefficient of

$$h_{gap,rad} = \frac{\sigma_{SB}}{\frac{1}{\varepsilon_{e,f}} + \frac{1}{\varepsilon_{e,s}} - 1} \left(T_{fuel}^2 + T_{sheath}^2 \right) \left(T_{fuel} + T_{sheath} \right)$$
 (6)

where is σ_{SB} the Stefan–Boltzmann constant and ϵ_e is the effective emissivity of the fuel and sheath.

1.3 Deformation Mechanics

In the reactor, the geometry of the fuel elements deforms as a result of a number of processes including: mechanical loading, thermal-expansion, material creep, fuel densification and fission product swelling. The FAST model assumes that the net deformation can be calculated as the sum of the individual strains.

1.3.1 Thermal Strain

The strain in a material due to thermal expansion, ε_{thm} , is approximated as

$$\varepsilon_{thm} = \alpha_P \left(T - T_0 \right) \tag{7}$$

where α_p is the thermal expansion coefficient as a function of temperature, T is the temperature and T_0 is the reference temperature for which the thermal strain is assumed to be zero.

1.3.2 Elastic Deformation

The FAST code includes two models for calculating deformation due to mechanical loading. The first model is the standard isotropic linearly-elastic (Hookean) model. According to this model, the linear strain, ϵ , and the shear strain, γ , are proportional to the applied stresses, σ and τ , respectively. The second model is a modification of the Hookian model to account for the presence of circumferential cracks in the pellet. In this model, the terms in the constitutive matrix which correspond to the hoop direction have been zeroed (effectively zero Young's Modulus and Poisson's ratios in these directions). In matrix form the modified relationship is

where, E and v are the Young's modulus, Poisson's ratios and the subscripts on the stress and strain indicate the appropriate direction vectors. This model is designed to capture the upper bound on the effect of cracking (similar to a shell relocation model) while still attempting to predict circumferential ridging.

Although it is known that the elastic properties of the fuel sheath are not isotropic, the total elastic strains are small compared to the plastic deformations which result from the effect of creep [13]. This makes the elastic anisotropy insignificant and thus the sheath was modelled as isotropic.

Contact between the pellet and the sheath is modelled using the penalty method to apply a force to the sheath in the radial direction. This force was not applied to the pellet because a very high Young's Modulus of UO_2 would result in negligible elastic strains. Pellet-to-pellet contact is considered only in the context of pellet-to-end cap interaction. In this case, it is assumed that the sheath will deform elastically to accommodate the pellet stack (producing an axial sheath stress that may lead to axial creep).

1.3.3 Pellet Densification and Fission Product Swelling

Densification strains were modelled using an empirical correlation developed by Hastings [14] for CANDU fuel. In this model, the volumetric strain is equal to

$$\varepsilon_{vol,dens} = \frac{\Delta V_{dens}}{V_0} = \frac{1 - p_0}{1 - p_0(1 - F)} - 1 \tag{9}$$

where p_0 is the initial porosity and F is the fraction of initial porosity which has been removed from the fuel. This is given by

$$F = 0.6 - \exp\left(-0.506 - 8.67 \times 10^{-10} T^3 \left(1 - \exp\left(-2.867 \times 10^{-2} Bu\right)\right)\right)$$
 (10)

where T is the temperature in Kelvin and Bu is the burnup of the fuel in MW h kgU⁻¹. According to this model, the fraction of initial porosity which can be removed from the fuel saturates at 60%.

The fission product swelling effect is divided into two sources with different mechanisms: solid fission product swelling and gaseous fission product swelling. The solid-fission product swelling occurs because the space occupied by two fission product atoms in the fuel matrix is greater than the space occupied by a single UO₂ atom. The volumetric strain due to solid fission product swelling is assumed to be linearly proportional to the fuel burnup. Olander suggests a volumetric strain of

$$\varepsilon_{vol,SFP} = 0.0032 \frac{Bu}{225} \tag{11}$$

where Bu is the burnup in units of MWh kgU⁻¹ [15,16].

The gaseous fission product swelling is caused by the formation of fission gas bubbles on the grain boundaries. The MATPRO [16] correlation for the volumetric strain rate of the gaseous fission products, $\varepsilon_{\text{vol},\text{GFP}}$, in units of s⁻¹ in differential form is calculated by

$$\frac{d(\varepsilon_{vol,GFP})}{dt} = 9.42 \left(10^{-36}\right) (2800 - T)^{11.73} e^{\left[-0.0162(2800 - T) - 8.0\left(10^{-27}\right)Buf\right]} \frac{dBuf}{dt}$$
(12).

Here Buf is the fuel burnup measured by number of fissions per unit volume.

1.3.4 Sheath Creep

Sheath creep occurs through a number of different mechanisms that are related to combinations of temperature and stress regimes. In FAST this was broadly divided into a low-temperature domain below 700 K and high-temperature domain above (based on the range of applicability of the high temperature creep model used). The creep rate in the low temperature domain was taken from the MATPRO 11 correlation [17], which divides it into thermal and irradiation creep terms. In the high-temperature regime the NIRVANA creep model developed by Sills and Holt of AECL was used [13,18]. In this model, the creep rate is the sum of grain boundary sliding, dislocation creep and transition creep. It accounts for retarding effects of the crystallographic dislocations on the creep rate through an internal stress. It also accounts for the anisotropy of the sheath due to the crystallographic texture using Hill anisotropy parameters.

1.4 Fission Gas Release Calculation

The release of fission gas from irradiated UO_2 fuel to the free volume in the element is a very complicated phenomenon. The model used in this work is based on that employed in reference [11]. The release process is modelled in two steps. In the first step, fission gas is produced in the fuel grains and diffuses to the grain boundary, where it accumulates forming intergranular bubbles. The second step occurs when the intergranular bubbles grow large enough to interconnect and release gas to the free volume of the element.

1.4.1 Release to the Grain Boundaries

The fission gas release to the fuel grains can be modelled by Booth diffusion of the fission gas to the fuel surface [10,11,19–21]. In this model, the fuel grains are treated as idealized homogenous spheres from which the fission gas atoms exhibit Fickian diffusion (where the particle flux is proportional to the concentration gradient). The fission gas is produced uniformly throughout each of the spheres, which are assumed to be initially free of the gas. The grain surface is assumed to be a perfect sink (i.e., fission gas concentration on the grain surface is zero). The atoms diffusing across the grain surface enter the intergranular bubbles.

The fission gas diffusion in the grains was implemented as a separate two-dimensional Cartesian geometry to represent the fuel grains which is coupled to the pellet model. In this geometry, the x-coordinate corresponds to the radial coordinate of the pellet model and the y-coordinate corresponds to the nondimensionalized radial coordinate within each fuel grain. This numerical implementation was validated against the analytic solution to this model (for step changes in model parameters) published by both Kidson [22] and by Rim [23]. The release rate to the grain boundary, R_{gb}, is

$$R_{gb}(t) = \frac{12}{g_d^2} D \frac{\partial C}{\partial y}\Big|_{y=1}$$
 (13).

where, g_d is the local fuel grain diameter, and D is the diffusion coefficient for fission gas in the UO₂ crystal matrix. This diffusion coefficient was obtained from Morgan [11] who followed the work of Turnbull *et al.* [24–26] and White & Tucker [21]. The average local UO₂ grain size was determined by solving the grain growth relationship provided by Khoruzhii et al. [27]. The rate of grain growth in m s⁻¹ is given as

$$\frac{dg_d}{dt} = 1.46 \left(10^{-8}\right) \exp\left(\frac{-32100}{T}\right) \left(\frac{1}{g_d} - \frac{\exp\left(\frac{7620}{T}\right)}{2.23 \times 10^{-3}} - \frac{F_{rate}T \exp\left(\frac{5620}{T}\right)}{6.71 \times 10^{18}}\right)$$
(14).

Here T is the temperature in K and F_{rate} is the fission rate density. Note that this model does not consider the distribution of grain sizes within a region; it only considers the average grain size. It was shown that this simplification produces good results for fission gas release despite potentially wide variations in the grain-size distribution [10].

1.4.2 Gas Release to the Fuel Element

Once fission gas has been released to the grain surface, it becomes trapped in intergranular bubbles between fuel grains. The amount of gas required at the grain surface to achieve interlinkage is the grain-boundary saturation, G_{bsat} . This effectively contains a portion of the fission gas on the grain boundary, G_b , in intergranular bubbles even after the bubbles have been interlinked. This is because if there is not sufficient fission gas to maintain the interlinked network, the bubbles become isolated and cannot release gas to the free volume. The kinetics of the release from the grain boundary is poorly understood. For simplicity, a first-order kinetic

12th International Conference on CANDU Fuel

Holiday-Inn Waterfront Hotel Kingston, Ontario, Canada, 2013 September 15-18

model has been implemented in FAST. According to this theory, the release rate from the grain boundary from a small fuel volume, δV , is

$$\frac{\partial R_e}{\partial V} = \begin{cases} \frac{G_b - G_{bsat}}{\tau_{fg}} & G_b \ge G_{bsat} \\ 0 & G_b < G_{bsat} \end{cases}$$
 (15)

where τ_{fg} is the time constant of fission gas release (user input). The release rate of gas atoms to the element, R_e , can then be calculated by integrating over the volume.

1.5 Gas Pressure Calculation

The internal gas pressure is calculated using the non-homogenous temperature form of the ideal gas law. This is given by

$$P = \frac{nR_{gas}}{\int_{V} \frac{1}{T} dV}$$
 (16)

where n is the number of moles of gas within the element, R_{gas} is the ideal gas constant and V is the volume occupied by the gas. In the model, the gas volume is divided into sub-volumes which are all calculated individually and added together. Since the gaseous regions are not meshed, the temperature in these regions has been approximated using the temperatures on the boundaries of the gas volumes. This converts some of the volume integral into boundary integrals.

2. Validation Procedure and Results

The FAST code has undergone a proof of concept validation against both experimental data and results obtained from the ELESTRES and ELOCA fuel performance codes. It should be stressed that this validation is intended to demonstrate the potential of the modelling technique. It is not intended to be compared to the industry recommended validation requirements for use in safety and licensing analysis. The validation of the FAST code has been done in two separate parts using experimental data provided by Atomic Energy of Canada Limited, Chalk River Laboratories.

The first validation exercise is a comparison of the predicted end-of-life condition of seven irradiated fuel elements which underwent post-irradiation examination (PIE). The cases were selected to cover a range of power, burnup and geometries. The maximum linear power and burnups for these cases ranged from 25 to 53 kW m⁻¹ and 132 to 552 MWh kgU⁻¹, respectively.

The PIE provided measurements of the fission gas release volume, grain size, sheath strain, and circumferential ridge heights of each element. These irradiation tests have integrated many different phenomena, which makes it difficult to attribute any discrepancies in the results to a specific model or phenomenon. The temperature in these tests was also too low to initiate any high-temperature effects.

The results of this comparison exercise have been summarized using the case number on the horizontal axis as illustrated in Figure 1. The average experimental value has been included along with the maximum measured value for each element. This provides a sense of scattering in the experimental results. The FAST calculation was performed with and without the incorporation of a circumferential crack model.

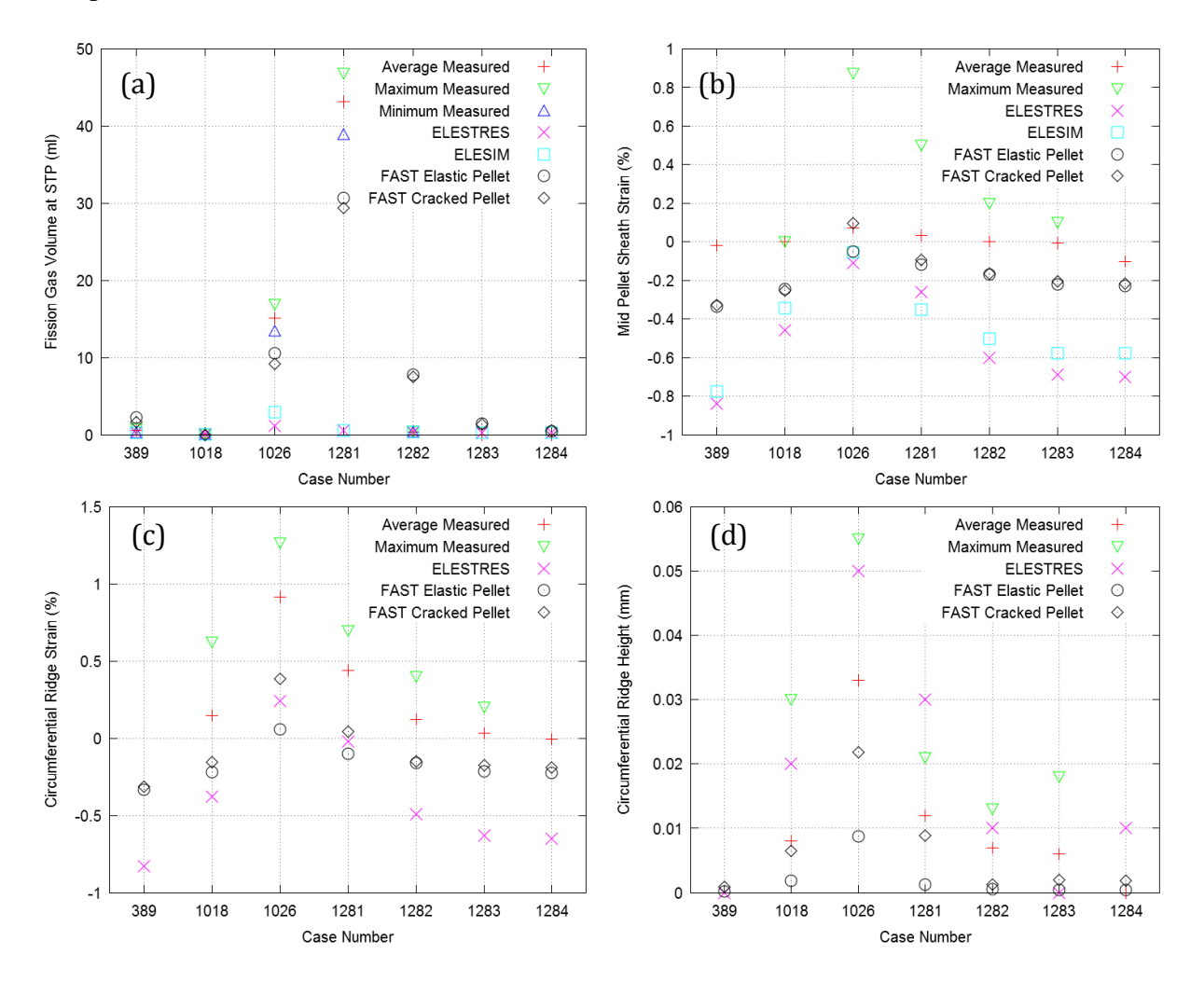


Figure 1 FAST validation for normal operating conditions showing (a) the fission gas release, (b) mid-pellet sheath strain, (c) circumferential ridge strain and (d) circumferential ridge height benchmarked against average and maximum measurements as well as the ELESTRES and ELESIM codes.

The second validation exercise was to validate the high-temperature transient components of the model. This was done by comparing model predictions to measurements from an irradiated fuel experiment, FIO-131, conducted at CRL to support fuel model validation [28]. This data was previously released to the Nuclear Energy Agency of the Organization for Economic Cooperation and Development (NEA-OECD) [29]. In the experiment, the primary coolant loop of an instrumented fuel element was depressurized during high power operation thereby simulating Loss Of Coolant Accident (LOCA) conditions. This data set includes in-reactor, time-dependent measurements of pellet and sheath temperatures, internal gas pressure and external coolant

pressure. A post irradiation analysis provided measurements of the sheath deformation and Zircaloy oxidation behaviour.

The FIO-131 experimental results showed significant axial dependence due to thermal hydraulic and neutronic effects along the length of an element. In the ELOCA code, this was accounted using an axial segmentation feature to divide the element into three parts. This capability, however, is not currently supported in the FAST code. The element was therefore modelled as three independent elements each representing a third of the experimental element (with no communication between these segmented elements). An additional case was also investigated in which the experimentally measured internal gas pressure was taken as an input parameter instead of being calculated. These results are illustrated in Figure 2.

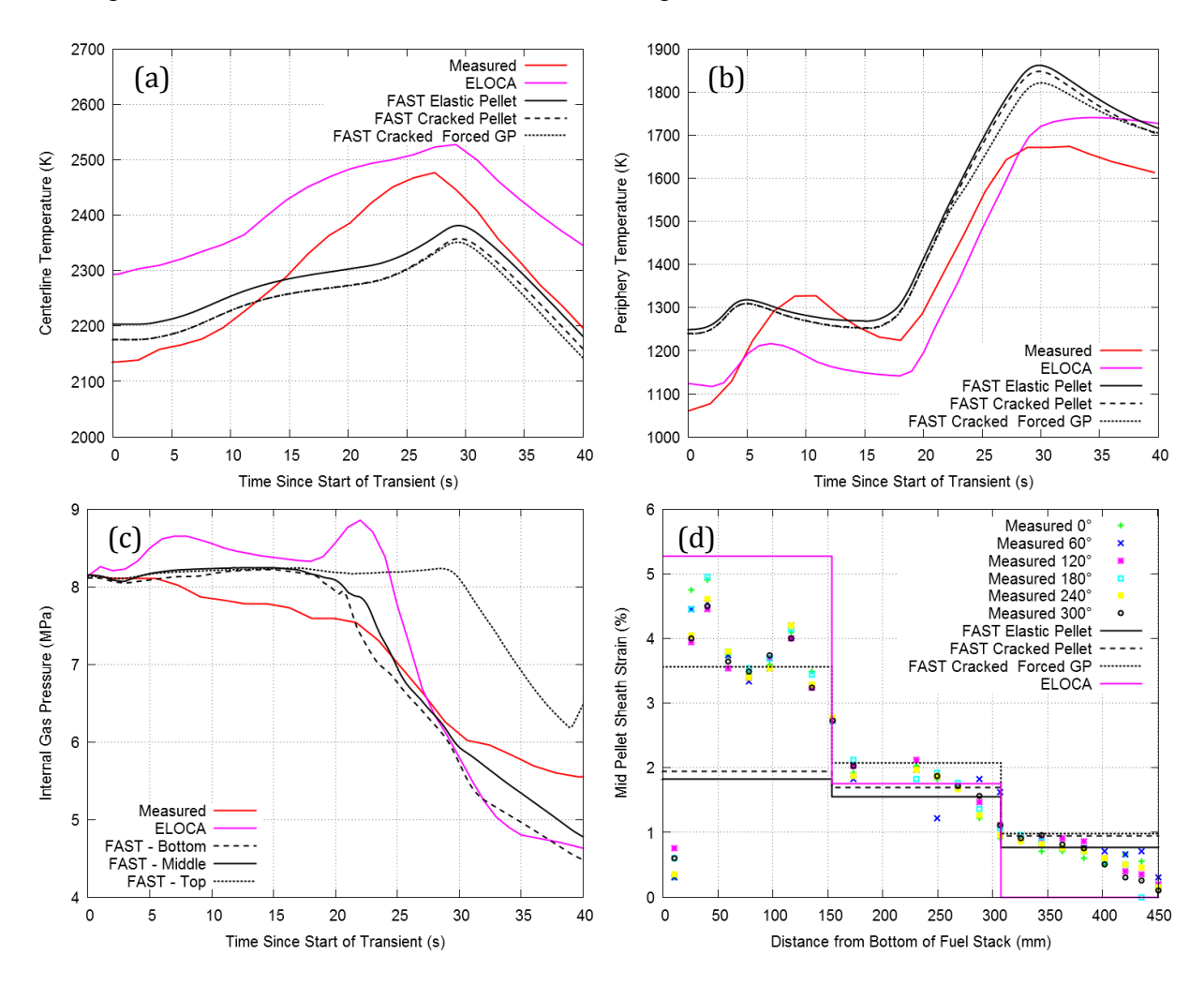


Figure 2 FAST validation for normal operating conditions showing (a) the fuel centerline temperature, (b) fuel periphery temperature, (c) internal gas pressure and (d) mid pellet sheath strain benchmarked against average and maximum measurements as well as the ELESTRES and ELESIM codes.

3. Discussion

Under NOC conditions (see Figure 1), the FAST code shows generally shows equivalent, or better, agreement with the experimental data than the existing IST code (ELESTRES), with some exceptions. The FAST code predicts larger fission gas release volumes than the ELESTRES and ELESIM codes for all cases. This prediction is an improvement in the two cases 1026 and 1281 (which showed significant gas release), however, it resulted in an over prediction of gas release in case 1282 (with case 1283 also indicating a similar trend although with lower burnup and power). Thus, the FAST code may overpredict fission gas release at low burnups (low fission gas release), but shows improved predictive ability at higer burnups (high fission gas release). The cracked pellet model is found to predict slightly lower fission gas release. This result is believed to be caused by increased pellet to sheath interaction, which leads to improved gap heat transfer. This in turn results in lower pellet temperatures, thereby reducing the diffusion of gas atoms in the lattice, and thus trapping more gas atoms in the pellet.

The predicted sheath hoop-strain at the mid-pellet and pellet-to-pellet interface show, particularly when using the cracked pellet model. This trend also exists for the circumferential ridge strain results. However, in virtually all cases, all of the models are consistently underpredicting the measured strains. The ridge height prediction from the FAST code (cracked pellet) was found to be closer to the mean measurements in five of the seven cases. In general, FAST was found to under-predict the ridge heights, while ELELSTRES over-predicted the average measured values.

In the transient test (see Figure 2), the FAST predictions agree well with the experimental results for both the centerline and fuel periphery temperatures. Since the modelling with the FAST code was performed assuming independent elements with no communication, it predicted different values of the internal gas pressure. For the bottom and middle segments, the gas pressure was found to fall below the measured values as the sheath expands (cracked pellet model results shown). Conversely, the internal gas pressure for the top segment is too high. These predictions can be explained as there is no communication between the segments.

As the radius of the sheath expands due to creep, the free volume in the element increases, which decreases the internal gas pressure. Since the bottom segment (with the largest increase in volume) calculates the pressure as if the whole element undergoes the same deformation, it would over predict the volume increase and under predict the pressure. Since the internal gas pressure acts as a driving force for deformation, this results in an under-prediction of the sheath creep. This theory was tested by using the internal gas pressure as an input variable; the results are labelled "Fast Cracked Forced GP". This calculation showed a significant improvement in the sheath strain predictions for the bottom segment, suggesting that the strain discrepancy was caused by the gas pressure calculation.

Two methods to improve the predictive capability of the FAST code for elements with strong axial variation have been identified. The first possibility is to develop axial segmentation with communication between the segments. This method is computationally efficient and straight forward to implement for a specific number of segments. However, the current format of the FAST code (using the COMSOL GUI) cannot be adapted to the general case with an arbitrary number of axial segments via text input making this solution somewhat unsatisfactory. The

second method is to extend the FAST code for modelling whole elements in two-dimensions. This would allow for the modelling of a complex axial dependence. This is more desirable, but also more computationally expensive. Both of these methods are currently being investigated.

4. Conclusions

Results from the proof of concept validation of the FAST fuel performance code were presented for both normal and transient reactor conditions. The NOC results demonstrated an improved predictive capability as compared to the ELESTRES code, particularly for the prediction of sheath strain. The transient test demonstrated a successful continuous transition from NOC to accident conditions. The model showed good agreement with pellet temperature measurements; however, the lack of support for modelling a strong axial dependence resulted in poor predictions for the internal gas pressure. This resulted in a large under-prediction of the sheath deformation in the highest-temperature region. An investigation into improving the model for a strong axial dependence is underway.

5. Acknowledgements

The authors would like to acknowledge the support of our colleagues at RMC, as well as J. Baschuk, B. Leitch, A. Williams, S. Yatabe and M.R. Floyd (AECL) for assistance and providing validation data. Funding for this work was provided by NSERC, UNENE and COG through the Industrial Research Chair (IRC) program and an ORF grant.

6. References

- [1] K.J. Gelhood, W.G. Luscher, C.E. Beyer, FRAPCON-3.4: A Computer Code for the Calculation of Steady-State Thermal-Mechanical Behavior of Oxide Fuel Rods for High Burnup, (2011).
- [2] M. Tayal, Modelling CANDU Fuel under Normal Operating Conditions: ELESTRES Code Description, Atomic Energy of Canada Limited, 1987.
- [3] K. Hallgrimson, M. Tayal, B. Wong, R. Aboud, Recent validations of the ELESTRES code, in: Proceedings of the 3rd International Conference on CANDU Fuel, Canadian Nuclear Society, Chalk River, Ontario, 1992: pp. 5.53–5.65.
- [4] Electric Power Research Institute (EPRI), Fuel Analysis and Licensing Code: FALCON MOD01: Volume 3: Verification and Validation, Palo Alto, CA, 2004.
- [5] K. Lassmann, C.T. Walker, J. van de Laar, Extension of the TRANSURANUS burnup model to heavy water reactor conditions, Journal of Nuclear Materials. 255 (1998) 222–233.
- [6] K. Lassmann, TRANSURANUS: a fuel rod analysis code ready for use, Journal of Nuclear Materials. 188 (1992) 295–302.
- [7] Nuclear Energy Agency, FEMAXI-6, Thermal and Mechanical Behaviour of LWR Fuel Rods, Organization for Economic Co-operation and Development (OECD) Nuclear Energy Agency (NEA). (2011).
- [8] G. Hasen, C. Newman, D. Gaston, BISON: An Implicit Solution Framework for Fuel Performance Simulation, in: Sandia National Laboratories, Albuquerque, New Mexico, 2009.
- [9] R.L. Williamson, J.D. Hales, S.R. Novascone, M.R. Tonks, D.R. Gaston, C.J. Permann, et al., Multidimensional multiphysics simulation of nuclear fuel behavior, Journal of Nuclear Materials. 423 (2012) 149–163.
- [10] K. Shaheen, A mechanistic code for intact and defective nuclear fuel element performance, Royal Military College of Canada, 2011.

- [11] D. Morgan, A thermomechanical model of CANDU fuel, MASc Thesis, Royal Military College of Canada, 2007.
- [12] F.. Campbell, L.R. Bourque, R. DesHaies, H. Sills, M.J.F. Notley, In-Reactor Measurements of Fuel-to-Sheath Heat Transfer Coefficients between UO2 and Stainless Steel, Atomic Energy of Canada Limited, Chalk River, Ontario, 1977.
- [13] H.E. Sills, ELOCA: Fuel element behavior during high-temperature transients, (1979).
- [14] I.J. Hastings, L.E. Evans, Densification Algorithm for Irradiated UO2 Fuel, Journal of the American Ceramic Society. 62 (1979) 217–218.
- [15] D. Olander, Fundamental Aspects of Nuclear Reactor Fuel Elements, Us Dept of Energy, 1976.
- [16] SCDAP/RELAP5 Development Team, Volume IV: MATPRO -- A Library of Material Properties for Light-Water-Reactor Accident Analysis, Idaho National Engineering and Environmental Laboratory, Idaho Falls, Idaho, 1997.
- [17] EG&G Idaho, Inc., MATPRO 11: Handbook of Material Properties for use in the Analysis of light water fuel rod behavior, (1979).
- [18] H.E. Sills, R.A. Holt, NIRVANA: a high-temperature creep model for zircaloy fuel sheathing, (1979).
- [19] A. El-Jaby, A model for predicting coolant activity behavior for fuel-failure monitoring analysis, PhD Thesis, Royal Military College of Canada, 2009.
- [20] S. Beck, The Diffusion of Radioactive Fission Products from Porous Fuel Elements, Battelle Memorial Institute, Columbus, Ohio, 1960.
- [21] R.J. White, M.O. Tucker, A new fission-gas release model, Journal of Nuclear Materials. 118 (1983) 1–38.
- [22] G.V. Kidson, A generalized analysis of the cumulative diffusional release of fission product gases from an "Equivalent Sphere" of UO₂, Journal of Nuclear Materials. 88 (1980) 299–308.
- [23] Rim et al., Background and Derivation of ANS-5.4 Standard Fission Product Release Model, American Nuclear Society, 1981.
- [24] J.A. Turnbull, C.A. Friskney, J.R. Findlay, F.A. Johnson, A.J. Walter, The diffusion coefficients of gaseous and volatile species during the irradiation of uranium dioxide, Journal of Nuclear Materials. 107 (1982) 168–184.
- [25] C.A. Friskney, J.A. Turnbull, F.A. Johnson, A.J. Walter, J.R. Findlay, The characteristics of fission gas release from monocrystalline uranium dioxide during irradiation, Journal of Nuclear Materials. 68 (1977) 186–192.
- [26] J.A. Turnbull, C.A. Friskney, F.A. Johnson, A.J. Walter, J.R. Findlay, The release of radioactive gases from uranium dioxide during irradiation, Journal of Nuclear Materials. 67 (1977) 301–306.
- [27] O.V. Khoruzhii, S.Y. Kourtchatov, V.V. Likhanskii, New model of equiaxed grain growth in irradiated UO2, Journal of Nuclear Materials. 265 (1999) 112–116.
- [28] J.A. Walsworth, P.J. Fehrenbach, R.C. Spencer, Comparisons Between ELOCA Code Calculations and CANDU Fuel Behaviour under LOCA Conditions, in: Proceedings of the 6th International Conference on CANDU Fuel, Ottawa, Ontario, 1985.
- [29] Atomic Energy of Canada Ltd. Chalk River Laboratories, IFPE/CANDU-FIO-131, CANDU experiment FIO-131 Fuel Behaviour under LOCA Conditions, Nuclear Energy Angency (NEA) Organization for Economic Co-Operation, 2007.